INSTITUTE OF PHYSICS PUBLISHING MEASUREMENT SCIENCE AND TECHNOLOGY

Meas. Sci. Technol. **15** (2004) 1120–1128 PII: S0957-0233(04)75385-0

Microstructure fibres for optical sensing in gases and liquids

John M Fini

OFS Laboratories, Murray Hill, NJ, 07302, USA

E-mail: fini@ofsoptics.com

Received 16 January 2004, in final form 11 March 2004
Published 13 May 2004
Online at stacks.iop.org/MST/15/1120
DOI: 10.1088/0957-0233/15/6/011

Abstract

A novel water-core microstructure fibre design allows nearly ideal guidance for aqueous sensing applications. The total internal reflection by a microstructured silica–air cladding provides robust confinement of light in a fluid-filled core, if the average cladding index is sufficiently below the index of water. Numerical results show dramatically improved loss and overlap of light with the sample, compared to evanescent-field fibres, indicating a direct improvement of sensor performance. A strategy for the improvement of evanescent-wave gas sensors is also discussed.

Keywords: fibre sensors, microstructure fibres, speciality fibres, optical sensing

1. Introduction

Microstructure optical fibres (MOFs) have been studied with great interest recently, spurred on by the observation of supercontinuum generation and its impact on metrology [1]. The field is developing rapidly and promises dramatic advances in communications fibre [2, 3] and a variety of devices.

For several years, there has been discussion on using microstructure fibres for sensing applications [4–7] such as the detection of trace chemicals in gas or liquid samples. Early proposals offer preliminary designs with little theoretical or experimental evidence that sensor performance would be enhanced by a microstructure fibre. At the same time, various experiments provide compelling proof that light can be made to interact with fluid samples in a controlled way [8], and that these designs should be pursued further. It has been recognized that the common evanescent-field designs have low overlap of light with the sample—a flaw that must be overcome to fulfil the potential of microstructured sensor-fibres. This problem of low overlap has also been discussed for non-fibre evanescent-field waveguide sensors; in [9] overlaps (or 'interaction ratios') less than 1% were calculated for a planar waveguide sensor of aqueous dyes.

This paper presents improved designs of microstructure fibres for sensing applications, including detailed simulations of guidance properties. The following section and the appendix provide a review of some background concepts in optical sensing and microstructure fibre waveguides. Section 3 looks at evanescent-field sensor fibres, proposing strategies for achieving modest improvements in their performance. Section 4 presents the primary result of the paper, a family of water-core fibre designs that achieve nearly ideal performance, and have significant advantages over previous designs. We expect these water-core fibres will have an immediate impact on optical sensing, and look forward to developments in fabrication and input/output coupling to such fibres. Similar designs may also improve the performance of water-filled waveguides for optical power delivery [10].

2. Specialty fibres for sensing applications

Optical sensing systems are important for a variety of applications. In a typical optical sensor, a light source illuminates a sample and a signal is obtained from light detected in transmission, reflection, fluorescence, etc, indicating the composition of the sample. Multiple wavelengths can be used for the illumination or the detection, taking advantage of known spectroscopic features of the detected species. One configuration passes an *unguided* beam of light through a bulk sample using free-space optics. In this case, the fibre may play a secondary role transmitting power and information to and from the sensing element, but does not interact directly with the sample. In figure 1, we depict a

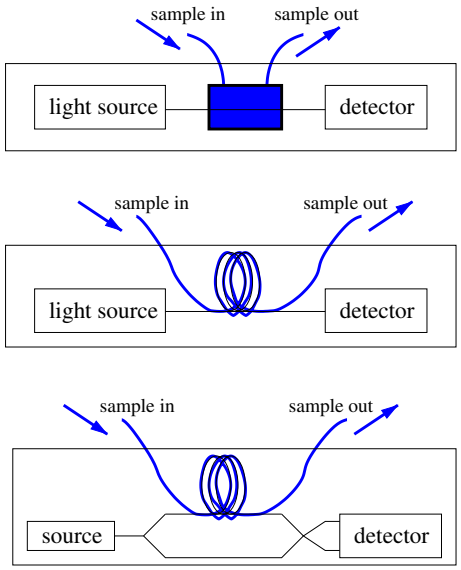

Figure 1. Optical fibre can dramatically improve the sensitivity of a sensor by increasing the interaction length between light and the sample. In a typical bulk configuration (top), light interaction with the sample may be limited to lengths of a few centimetres. We present specialty fibre designs that will allow interaction of guided light with a sample over a metre length and greater distances (middle). Interferometric detection of light (bottom) can also be used if mode-coupling in the waveguide can be controlled.

different kind of system, where light interacts with the sample as it is guided along a fibre or capillary waveguide. The measured signal can be enhanced by using long interaction lengths, difficult to achieve in bulk samples. Also shown is an interferometric detector, which may be used to construct ultra-high sensitivity detectors.

The guided-light approach is currently used in some sensing systems despite the poor performance offered by traditional low-index-core optical waveguides. These waveguides face a difficult material problem: metal waveguides have high loss at optical wavelengths, but index guiding (or total-internal reflection (TIR)) requires a 'cladding' material with lower index than the gas or liquid sample. Waveguides based on fluid-filled capillaries or glass (non-microstructured) fibres inevitably suffer high loss or low overlap of the field with the sample, or achieve low loss using a very large-core waveguide [10, 11]. The latter possibility brings limitations due to highly multimode propagation.

Microstructure fibres present novel and practical ways around these obstacles by providing a 'designer material' with reduced index, and introducing bandgap effects. Existing designs include the evanescent-field fibre, such as shown in figure 2, and bandgap-guided fibres. In this and other schematic cross-sections, the shaded circles represent holes that run along the length of the glass fibre. By pumping a sample material into the holes of such a fibre, we can bring it in contact with the guided light. The guidance mechanisms (bandgap and index-guidance) are defined in the appendix. Unlike very-large-core waveguides [10, 11], microstructure fibres can be designed to be single-moded, allowing interferometric detection and eliminating mode-coupling problems. Incorporating any of these designs into a sensing system should simply be a matter of providing fluid

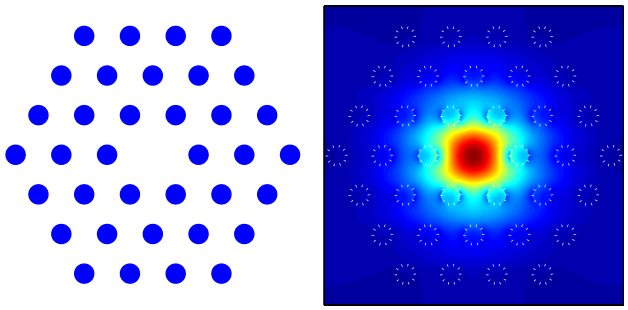

Figure 2. An evanescent-field microstructure fibre has holes running along the length of a glass fibre, near the light-guiding core region. A common cross-sectional geometry is the centre-hole omitted triangular-lattice (COT) type, shown left with holes shaded. The optical power (right) shows evanescent fields penetrating into the holes can interact with a gas or liquid sample for optical sensing.

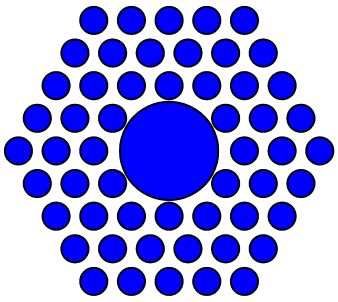

Figure 3. Fibres with the seven-hole adjoined triangular-lattice (SAT) geometry have been demonstrated as air-core bandgap waveguides with low loss and good confinement to the core air region.

and optical inputs, but many practical issues have barely been explored.

Air-core bandgap-fibre measurements demonstrate the basic requirements for a sensor fibre, particularly high overlap with a gas sample [3, 12]. These designs use a microstructured cladding but with a large central hole in the core, for example the seven-hole adjoined triangular-lattice (SAT) geometry of figure 3. While bandgap fibres are an interesting possibility for sensing and other applications, they come along with fabrication difficulties, and are generally less robust than index-guided MOF. Below, we show that a novel index-guided fibre type achieves high overlap without using bandgap guidance, and should therefore have advantages in manufacturability and robustness. In any case, the proposed index-guided watercore fibre is an interesting alternative to evanescent-field and bandgap fibres, and should be explored further.

2.1. Sensitivity, loss and overlap

By providing low loss and high overlap, a well-designed water-core fibre could directly improve sensitivity and optical power requirements of guided-light systems. While no single equation describes the many diverse optical sensors, the measured signal is often roughly proportional to interaction with the sample, and attenuated by the loss factor,

$$\text{Signal} \propto (\text{Interaction length}) \times (\text{Overlap}) \times e^{-\text{Loss}\times\text{Length}}. \quad (1)$$

This may result, for example, from small-signal analysis (relevant to the sensitivity) of an interferometric detection or optical absorption measurement. The signal enhancement obtained from a long interaction length is limited by the loss, and can be cancelled if the overlap is too small.

Overlap is most simply understood as the fraction of optical power that is exposed to the sample. Light in an evanescent-field fibre is primarily confined to the glass core (figure 2); it has little 'overlap' with a fluid sample in the holes, and proportionately small detected 'signal'. Overlap can be quantified by the shift in the index n_{eff} of the guided mode, which then leads to phase shifts or absorption (for imaginary n_{eff}-shifts). A precise formulation is standard perturbation theory for guided vector fields

$$\delta n_{\text{eff}} \approx \frac{\int \mathrm{d}A\, \Delta\epsilon |\boldsymbol{E}|^2}{2\sqrt{\epsilon_0\mu_0}\int \mathrm{d}A\, \mathcal{R}\{\boldsymbol{E}^* \times \boldsymbol{H}\}\cdot\hat{\boldsymbol{z}}}, \tag{2}$$

where $\Delta\epsilon = \Delta\left(n^2_{\text{sample}}\right)$ includes the index-shift and absorption of the bulk sample. Generally, a more intuitive formula is used,

$$\delta n_{\text{eff}} \approx \delta n_{\text{sample}} \frac{[\text{Power in fluid}]}{[\text{Total power}]}, \tag{3}$$

which is equivalent in the limit that the modes have moderate polarization effects.

2.2. Calculation of waveguide modes

The design of an effective fibre-optical sensor includes many aspects, and depends on the details of the sample and sensing environment. This paper focuses on the calculation and design of the relevant optical properties (primarily loss and overlap) of microstructure fibres. Single-mode or few-mode operation may be required in some systems, particularly if interferometric detection is being used. Other issues, such as getting light and fluids into the fibre, are crucial to a practical design, but are not discussed in detail here. The analysis uses an established numerical technique, the multipole method [13], to calculate characteristic modes of the fibre. These natural modes are defined as solutions to Maxwell's equations which are translationally invariant,

$$\boldsymbol{E}(\boldsymbol{r}) = \boldsymbol{E}(x, y)\exp(\mathrm{i}\beta z). \tag{4}$$

The mode calculation gives us the power distribution in the fibre cross section and the propagation constant $\beta = n_{\text{eff}}2\pi/\lambda$, indicating the optical phase (real β) and attenuation (imaginary β) that accumulates as light propagates.

3. Evanescent-field fibres

The design of evanescent-field fibres to maximize overlap was discussed in [6]. Figure 4 reviews the same basic trends (for somewhat different geometry, figure 2) with varying ratios d/Λ of hole diameter and spacing. Generally, overlaps are quite poor for small holes. Better penetration into the holes is obtained for longer wavelengths and larger d/Λ [6], but only up to a point, since large λ/Λ comes along with higher confinement losses. The loss plotted is for a three-ring cladding, and can naturally be reduced by adding more holes, but the trend indicates the weaker confinement at long wavelengths. Ultimately this, along with bending or fabrication constraints, will place a limit on the available overlap.

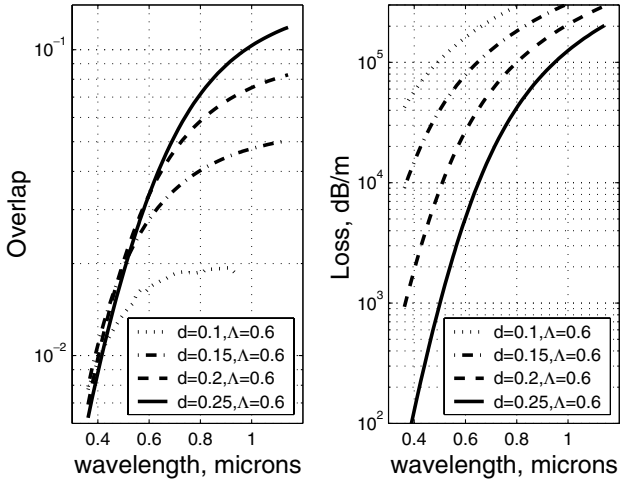

Figure 4. Overlap and loss for a family of evanescent-field silica–air fibres.

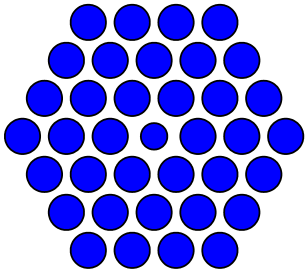

Figure 5. Modified evanescent-field geometry.

3.1. Improved evanescent-field design

There is huge flexibility in adjusting the sizes, shapes and positions of the microstructure holes to optimize performance. One generalization of the evanescent-field fibre is shown in figure 5. Rather than introducing a core defect by eliminating one hole entirely from the lattice, we use a hole of reduced diameter, $d_{\text{core}}/d < 1$. By adding the centre hole where we expect the fundamental mode power to be highest, we aim to force more of the optical power to overlap with the gas. This design principle could be generalized to more complex structures.

Simulation results of figure 6 confirm that the overlap of the modified design can be dramatically higher than the corresponding solid-core structure (with $d_{\text{core}} = 0$) at a given wavelength. But at fixed wavelength (and fixed d, Λ), the modified designs give both higher overlap and higher confinement loss, complicating the results. To make a more fair comparison, figure 7 replots the same results as overlap versus loss. There, it is clear that the modified design improves overlap for a fixed loss level, as well as for fixed wavelength. The practical impact of this strategy should be explored further.

Since these fibres are index-guided, we expect robust guidance as long as the defect is sufficiently pronounced. Clearly, as d_{core}/d approaches 1, accidental variations in the lattice will cause large changes in the guidance properties. While these overlap improvements are interesting, the modified-evanescent design still has potential problems which should be investigated. For example, the centre hole may complicate input/output coupling from standard fibre

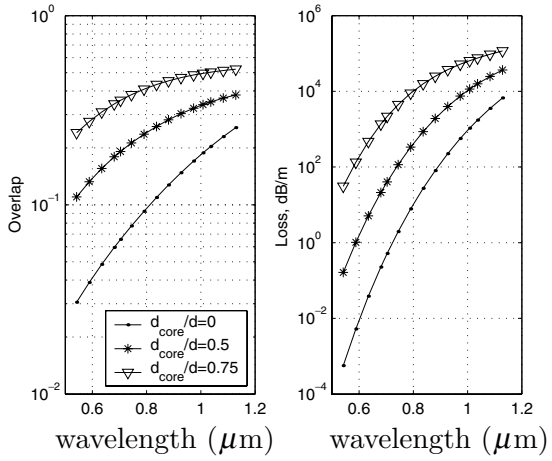

Figure 6. Modified evanescent-field fibre overlap.

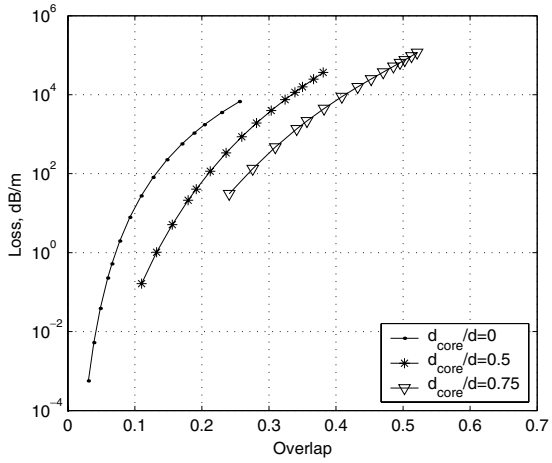

Figure 7. Modified evanescent-field fibre overlap plotted versus loss.

(although an adiabatic mode converter would, in theory, provide efficient coupling).

4. Water-core fibres

We now turn to sensing in aqueous media. On the one hand, the basic problem is similar, and the same types of design can be used as for gas sensors: evanescent-field or bandgap fibres. The principles are exactly the same, but the details must include the material properties of water. On the other hand, since the index of water is considerably higher than that of air, a very different kind of design is also possible: index-guidance in a water core using a silica–air cladding.

Before we discuss three-material fibres, we note a recent variation on the evanescent-field fibre theme [7], based on index-guiding in the many glass webs of a microstructure fibre. While the basic fibre geometry is similar to the design proposed here, the absence of air from the cladding makes a large difference in guidance properties and performance. Using cladding-modes in a large-d/λ SAT geometry (similar to those used for air-core guidance), this work should allow fairly high optical overlap, but with the disadvantage that light tends to localize at any irregularities of the cladding. The highly multimode, very irregular output field pattern will limit sensor applications unless the fabrication is extremely precise.

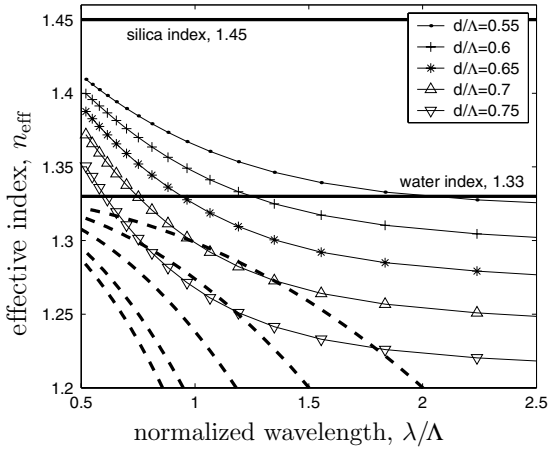

Figure 8. For high enough air-fill-fraction, the average index of a silica–air cladding can drop below the index of water, allowing index-guidance of light in a water core. The average index is here quantified by the wavelength-dependent total-internal-reflection edge, $n_{\rm TIR}(\lambda)$, which crosses $n_{\rm water} \approx 1.33$ for all d/Λ greater than around 0.54. Also shown are analytical mode line estimates (dashed), suggesting that strong confinement of light in the water core will require d/Λ values closer to 0.7.

4.1. Basic design

By surrounding a water core with an air–silica microstructured cladding, it is possible to achieve robust index guidance, well confined to the core and with high overlap with the sample. Such structures can be designed to be many-moded, few-moded or single-moded, as required by the measurement system. This strategy can be implemented in a SAT fibre (figure 3) for example, starting from simple, approximate design rules which follow directly from the basic waveguide principles discussed in the appendix. The intuitive design is then followed by detailed numerical simulation using the multipole method.

In order to achieve robust confinement in a water core, the 'average' index of the air–silica cladding must be below the index of water, $n_{\rm water} \approx 1.33$. Intuitively, this average index will be low enough when the air fill fraction (proportional to $(d/\Lambda)^2$) is high, and for sufficiently long normalized wavelength λ/Λ. The condition can be quantified using the standard Bloch-wave analysis of the lattice (see, for example [13, 14]); this gives the index $n_{\rm TIR}(\lambda)$ above which light can be guided through total internal reflection, or 'index-guidance' (see also appendix). Figure 8 shows $n_{\rm TIR}$ as a function of λ/Λ for several values of d/Λ. For simplicity material dispersion has been neglected in this calculation: $n_{\rm hole} = 1$ and $n_{\rm silica} = 1.45$. As expected, for larger holes ($d/\Lambda \gtrsim 0.54$) and long wavelength we see the basic requirement for guidance satisfied: the water index falls within the TIR-confinement region. This requirement can be refined if we assume that light must be well confined to a core of appropriate size; as discussed in the appendix, a crude mode index approximation (A.3) is

$$n^2_{\rm eff,fund} = n^2_{\rm core} - 0.32(\lambda/D_{\rm core})^2. \qquad (5)$$

for the fundamental mode, with core diameter $D_{\text{core}} \approx 2\Lambda$ for a SAT geometry. Similarly, one would expect a higher-order mode near

$$n^2_{\text{eff,HOM}} = n^2_{\text{core}} - 0.58(\lambda/D_{\text{core}})^2. \quad (6)$$

The analytical mode-line estimates have been drawn in figure 8 for fundamental and higher-order modes. From the figure, we expect that $d/\Lambda \gtrsim 0.7$ is required to obtain a well-confined fundamental mode, and $d/\Lambda \lesssim 0.8$ is required if a single-moded or few-moded waveguide is desired. This suggests a range of preferred air-fill fractions as a starting point in our design. Smaller values would have less well-confined modes (and worse overlap and loss), and larger values may have problems associated with multiple modes and fabrication difficulties.

This type of fibre would offer key advantages over evanescent-field designs. The major challenge in implementing real sensors is to couple (simultaneously) fluids and light into the fibre—a problem not only for this fibre class, but for bandgap and evanescent-wave fibres as well. Because the core hole is much larger than the cladding holes, one will automatically achieve different fill rates using capillarity or active pumping of fluids, allowing one to selectively fill the core hole, or selectively plug the cladding holes. For applications where continuous loading of the sample is required, the simplest conceptual scheme would couple light into the core using a lens immersed in the sample, in essentially the same way that free-space optics are used to couple light into standard glass fibres. For other applications, there may be advantages to sealing the fibre by plugging or collapsing the core hole before measurement. The inherent scalability of the fibre drawing process, where the natural production lengths are thousands to millions of metres, raises the possibility of fibre as an inexpensive consumable. This would have obvious advantages regarding contamination.

4.2. Numerical simulation

The qualitative description is very nicely born out numerically, with a few complications. Figure 9(*a*) shows the effective index for several modes of a preliminary waveguide design. The fibre has three rings of holes with $d = 0.76\,\mu$m, $\Lambda = 1\,\mu$m and one large circular core hole with diameter $2.27\,\mu$m. Material dispersion for silica and water was included in these and the following calculations. As expected, for wavelengths above $0.7\ \mu$m, the condition $n_{\text{eff}} < n_{\text{water}}$ is satisfied and a mode emerges with power primarily confined to the core (shown in figure 9(*b*)). However, two other types of modes appear in this waveguide, and can complicate the design: first there are the poorly-confined, relatively high-loss cladding modes with n_{eff} just below the TIR region. These have power distributed through the cladding region, as in figure 9(*c*), and are analogous to more familiar cladding modes of standard fibres or solid-core microstructure fibres, discussed previously in [15, 16]. Finally there are 'web' modes with power localized in the glass web near the core (figure 9(*d*)), similar to surface modes of air-core fibres [17].

Cladding modes are not of practical importance in the fibre as long as two conditions are met: they are much higher loss than the confined modes (true for the simulated fibre of figure 9), and coupling between the confined modes and

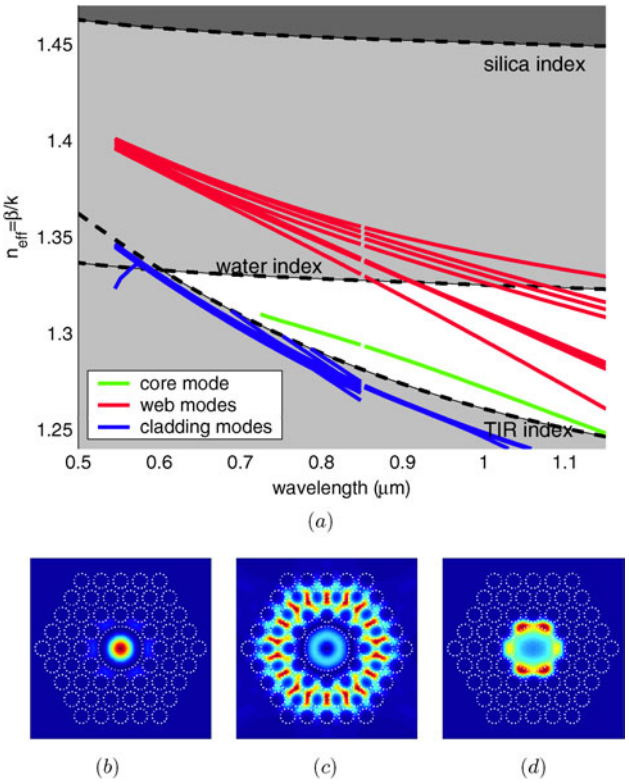

Figure 9. The water-core fibre with air–silica cladding supports the desired fundamental core mode (circle), but also cladding modes (stars) and modes guided in the glass webs surrounding the core (dots). Below, optical intensity profiles at $\lambda = 1\ \mu$m are shown for modes representative of these three types, (*b*), (*c*) and (*d*), respectively. Losses for the web-guided modes can be small, and so controlling these modes is an important part of fibre design.

cladding modes, for example by microbends, is sufficiently small. Web modes have been discussed with respect to air-core fibres [7], and can be problematic, in particular since they can have lower losses than the core modes. As we will see, it is possible to eliminate these unwanted modes, for example by adjusting the geometry of the core region [18].

The intensity profiles of figure 9(*b*)–(*d*) highlight that some modes are readily identifiable as core, cladding or web-modes, but this distinction is not always black-and-white. 'Core' modes have some power in the web and cladding regions, and may emerge continuously from web or cladding modes as wavelength is increased.

4.3. Reduced-web water-core fibre

We have explored an improved design, where the glass web around the core is perforated in order to remove unwanted glass-guided modes. This strategy was successful, and gave the essentially ideal guidance properties described in figures 10, 11 and 12. Circular-hole perforations were used for numerical reasons, but other reduced-web geometries should give equivalent results, and may be chosen on the basis of manufacturability. The first two figures use $\Lambda = 0.9\,\mu$m, $d = 0.648\,\mu$m and centre hole diameter $2.35\,\mu$m. It shows essentially single-moded behaviour, indicated by the high cladding-mode losses and the absence of the web modes.

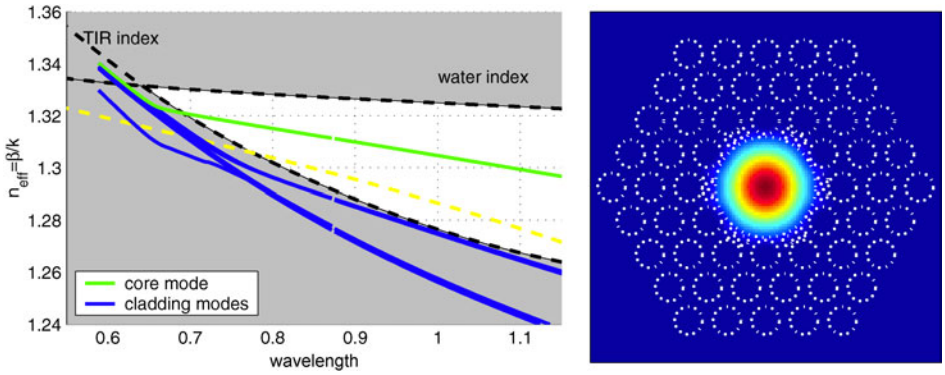

Figure 10. By sculpting the glass in the vicinity of the core, single-moded operation can be achieved in the index-guiding region. In the left-hand plot, we see a single-mode line light grey in the unshaded guidance region between water index and the TIR edge. In the right-hand plot, we see the intensity of the fundamental mode, almost completely confined to the water core of this modified SAT fibre. Dotted lines indicate the holes.

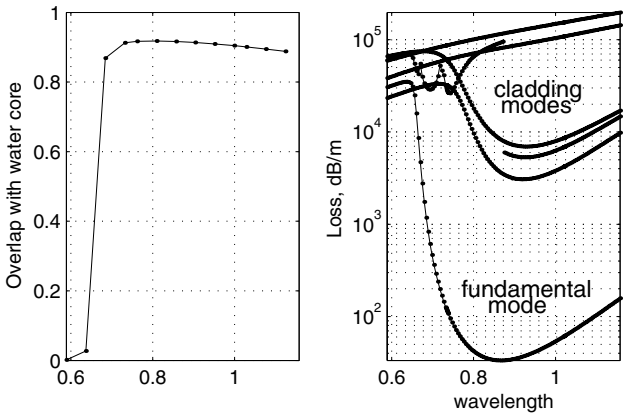

Figure 11. Overlap (left) and loss (right) of the reduced-web silica–air–water fibre are shown. As the average cladding index drops below that of water, the fundamental core mode emerges with an abrupt increase in core overlap and abrupt drop in loss.

The design of figure 12 uses $\Lambda = 1.0\,\mu$m, $d = 0.76\,\mu$m and centre hole diameter 2.57 μm, and is designed to include two groups of core modes: the fundamental and the first higher-order-mode group. For both the single-moded and few-moded designs, propagation is achieved over a wide range of wavelengths, and at wavelengths useful for some sensing applications. Figure 11 confirms that the fundamental core mode has high overlap and much lower loss than the cladding modes.

Figures 10 and 12 also include (dashed) the analytical mode-line estimates given by equations (5) and (6). Quantitative agreement with exact results is not expected, but the simple predictions do provide a useful, rough guideline to guide simulations. Further, the power and field profiles for core modes can easily be identified with modes of traditional round waveguides, that is LP_{01} like, TM_{01} like, etc.

While some sensors rely on interaction of light directly with the fluid sample, the most chemically selective and sensitive sensors measure the reaction of the sample with an indicator material, for example, bound on a surface. A highly selective biosensor could be made by coating the surface of the centre hole with a receptor, whose reaction with the sample could be measured with high sensitivity. Higher-order core modes in a water-core fibre may have advantages for such systems, since the optical power in these modes can be concentrated near a glass–fluid interface, as seen in figure 12. Coupling of light between modes of solid few-moded fibres has been accomplished with excellent efficiency [19],

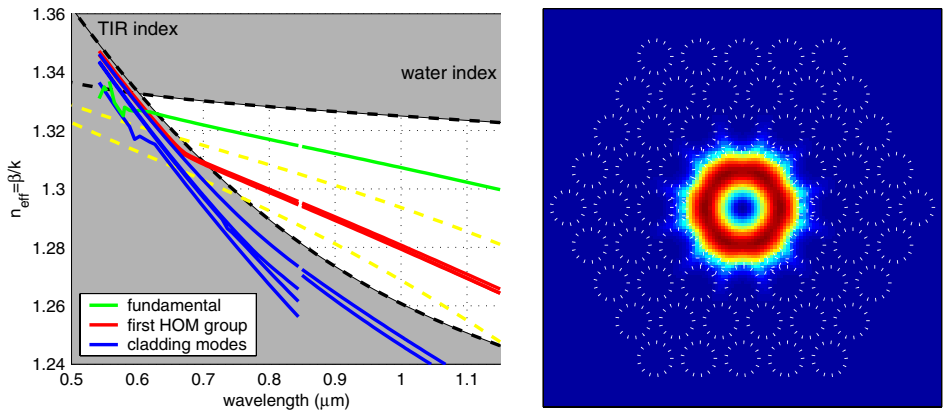

Figure 12. Another SAT fibre with reduced web includes the fundamental mode and one higher-order core-mode group. This should allow controlled coupling into modes with light concentrated at the glass–water interface. The intensity of a higher-order core mode is shown (right).

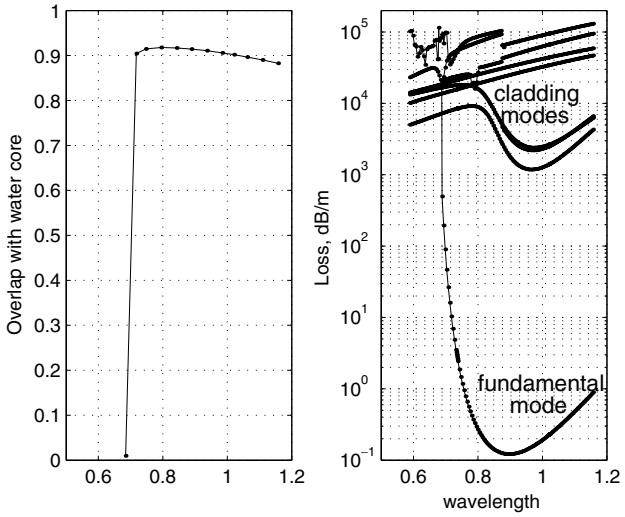

Figure 13. By increasing the number of cladding rings from three to five, we obtain low confinement losses for the fundamental mode, suitable for efficient sensing on metre-length scales. All other unwanted modes experience high losses, which can be beneficial in systems where multi-path interference is a problem.

and could allow direct or interferometric detection of light in these modes.

So far we have looked at three-ring structures for all designs. This allows for fast calculation, and puts all designs on an equal footing for 'fair' comparisons of confinement loss. Once a suitable three-ring design is obtained, one can easily achieve a desirable confinement loss level (with negligible change in the basic mode structure) by adding more holes to the cladding. In figure 13, for example, we show the loss and overlap of a five-ring design, otherwise identical to that of figure 10. Further loss reduction is easily possible, down to the limit of material losses: fibres with ten or more rings of holes are routinely fabricated, and the required total cladding diameter is quite reasonable. Absorption in water was not included in the calculation, but will become significant for five or more rings of holes, especially above 1100 nm. For the five-ring structure, the calculated confinement loss in the fundamental is below 1 dB m^{-1} over a wide wavelength range (750–1150 nm), while the unwanted higher-order modes (mostly cladding modes, but with some energy in the core) are far more leaky. These results demonstrate a nearly-ideal single-mode waveguide for aqueous sensing applications: the fibre combines almost complete overlap of light with the sample with acceptable loss over long interaction lengths. The well-shaped mode fields, robust confinement mechanism and relatively large core size present further advantages over previously proposed waveguides.

5. Conclusions

For sensors, as for other applications, microstructure fibres offer ways around the constraints of traditional waveguides. Novel strategies for microstructured sensor-fibre design have been proposed, with significant advantages over previously proposed evanescent-field and bandgap fibres. Specifically numerical simulations have demonstrated a single-mode water-core fibre with <1 dB m^{-1} loss and near-unity overlap with the sample over a wide wavelength range. This fibre would make a nearly ideal sensor waveguide, and should be robust to fabrication imperfections.

Detailed simulations for three particular water-core fibres have been presented along with qualitative design rules. Using the same basic strategy, fibres can readily be designed to accommodate different sample materials, interaction wavelengths, core sizes, etc, as required by the details of the application.

Acknowledgments

I thank Ryan Bise, Jeff Nicholson, Dennis Trevor, Samir Ghalmi and David DiGiovanni for support and useful discussions.

Appendix. Microstructure fibre principles

Appendix A.1. Confinement mechanisms: TIR and bandgap regions

In this section, we review some basic principles of confinement and guidance in microstructure fibres. Interestingly, the basic physical confinement mechanism is not the same for all MOF modes. One way to understand the mechanisms is to consider where a mode falls in the k–β plot, where $k = 2\pi/\lambda$ relates to the wavelength and β is the axial propagation constant defined by equation (4). Such a plot is shown schematically in figure 14. The simplest microstructure fibres are two-material structures with a high-index $n_{\rm hi}$ and low-index $n_{\rm lo}$ material, typically silica glass with vacuum holes. These two indices divide the plot into three regions, independent of the geometry of the core or cladding. The properties of waves in these regions are determined by the transverse-k-vector, $k_\perp^2 = k^2n^2 - \beta^2$, in the two material regions $n = n_{\rm hi}$ and $n = n_{\rm lo}$.

- For $\beta > n_{\rm hi}k$, electromagnetic waves are evanescent in both high- and low-index materials. That is, $k_\perp$ is imaginary for both $n = n_{\rm hi}$ and $n = n_{\rm lo}$, and no guided modes are possible.
- For $\beta < n_{\rm lo}k$, waves can propagate in both materials ($k_\perp$ is real everywhere), and so neither material can perfectly confine the waves. Index-guiding is therefore impossible and modes must be confined by bandgap effects.
- For $n_{\rm lo}k < \beta < n_{\rm hi}k$, waves propagate in high-index and are evanescent in low-index materials. Confinement is typically index-guided, but can involve bandgap effects as well.

Once the specific lattice geometry is known, we can go farther: Bloch-wave analysis identifies interesting regions where an infinite lattice would perfectly exclude light. These regions are shown as a broad total internal reflection region and narrow bandgaps in figure 14. The TIR region and bandgaps can be calculated numerically by several methods (including publicly available software [20]), using approximate formulae [21, 22], or simply the asymptotic long-wavelength limit (for air-fill fraction (AFF)):

$$n_{\rm TIR} \to (1 - {\rm AFF})n_{\rm glass} + {\rm AFF}n_{\rm air}. \qquad (A.1)$$

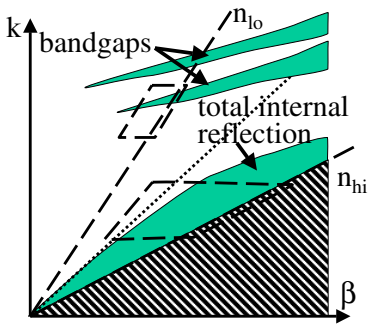

Figure 14. The k–β plot shows various confinement mechanisms at work in a two-material microstructure fibre. First, lines $\beta = n_{lo}k$ and $\beta = n_{hi}k$ divide the space into three regions: for $\beta > n_{hi}k$ no modes are possible (hatched region), for $\beta < n_{lo}k$ only bandgap confinement is possible, and for intermediate β, both bandgap and index-guiding confinement are possible. Bloch-wave analysis identifies the detailed confinement regions (shaded): where the lattice provides through total-internal reflection (broad TIR region) or bandgap confinement (narrow fingers). Regions of interest for further mode calculations are shown schematically as dashed boxes for air-core (upper box) and silica-core (lower box) fibre.

Most commonly, a MOF is one of two types: an index-guided fibre with high-index core, or a bandgap fibre with low-index core. In both cases, confined modes consist of propagating, sinusoid-like wave in the core region, and an exponential falloff in the cladding region. For a bandgap fibre, this falloff critically depends on the periodic structure of the cladding, since neither material alone exhibits exponential confinement. While index guidance in MOF is quite easy to observe, considerably more effort is required to observe low-loss air-core guidance [3].

Appendix A.2. Core modes and cladding modes

Generally, microstructure fibres have large index contrast, and thus display strong confinement of light to the core, at least for some modes at short wavelengths. It is useful to recognize that while MOF have unique properties, their mode structure is quite similar to traditional waveguides found in textbooks [16, 23]. MOF modes can even be compared (roughly) to the analytical mode solutions of a perfectly conducting waveguide of roughly the same dimensions. Using textbook solutions [24, p 180], boundary conditions require that the transverse $\boldsymbol{k}$-vector component k_{perp} and the core size D_{core} satisfy simple phase conditions: for the jth-order mode,

$$k_{\perp} D_{\mathrm{core}} = \frac{2\pi D_{\mathrm{core}}}{\lambda}\sqrt{n_{\mathrm{core}}^2 - n_{\mathrm{eff}}^2} = 2\pi C_j \qquad \text{(A.2)}$$

where the constants C_j depend on the specific geometry (slab, cylindrical, etc), and are of order one for the lowest modes. Microstructure fibres do not have simple 'constants' C_j independent of wavelength, hole size, etc, and require numerical computation. However, as long as a mode is well confined to the core, the qualitative behaviour of the effective index can be understood fairly well by analogy with the perfect-conductor analogy

$$n_{\mathrm{eff},j}^2 \approx n_{\mathrm{core}}^2 - (\lambda C_j / D_{\mathrm{core}})^2. \qquad \text{(A.3)}$$

By guessing values of C_j of the right order (for example, using a cylindrical perfectly-conducting waveguide analogy), we can obtain *a priori* estimates of the fundamental and higher-order mode lines.

Not all microstructure fibre modes display this strong confinement. Modes have also been calculated and observed [25] with power distributed through the cladding. For example, higher-order modes beyond cutoff were discussed in [15]. These modes also can be accurately approximated by an intuitive, quasi-analytical description [16]. In this description, a mode consists of six Bloch-wave components with Bloch vector magnitude k_{Bloch}. The approximate modal condition for a cladding with N rings

$$k_{\mathrm{Bloch}} D_{\mathrm{clad}} = \frac{3\pi(N+1)\Lambda}{\lambda}\sqrt{n_{\mathrm{TIR}}^2 - n_{\mathrm{eff}}^2} = 2\pi \qquad \text{(A.4)}$$

leads to a simple estimate of cladding-mode effective index

$$n_{\mathrm{eff},j}^2 \approx n_{\mathrm{TIR}}^2 - (2\lambda/3(N+1)\Lambda)^2. \qquad \text{(A.5)}$$

References

[1] Diddams S A *et al* 2000 Direct link between microwave and optical frequencies with a 300 THz femtosecond laser comb *Phys. Rev. Lett.* **84** 5102

[2] Johnson S G *et al* 2001 Low-loss asymptotically single-mode propagation in large-core OmniGuide fibers *Opt. Express* **9** 748

[3] Venkataraman N *et al* 2002 Low loss (13 db/km) air core photonic band-gap fibre *ECOC*

[4] Birks T A *et al* 1995 Full 2d photonic bandgaps in silica/air structures *Electron. Lett.* **31** 1941

[5] Monro T M, Richardson D J and Bennet P J 1999 Developing holey fibres for evanescent field devices *Electron. Lett.* **35** 1188

[6] Monro T M *et al* 2001 Sensing with microstructured optical fibers *Meas. Sci. Technol.* **12** 854

[7] Jensen J B *et al* 2003 Photonic crystal fiber based evanescent-wave sensor for detection of biomolecules in aqueous solutions *CLEO* p CTuP5

[8] Kerbage C *et al* 2002 Highly tunable birefringent microstructured optical fiber *Opt. Lett.* **27** 842

[9] Kang S W, Sasaki K and Minamitani H 1993 Sensitivity analysis of a thin-film optical waveguide biochemical sensor using evanescent-field absorption *Appl. Opt.* **32** 3544

[10] Diemer S, Meister J, Jung R, Klein S, Haisch M, Fuss W and Hering P 1997 Liquid-core lightguides for near-infrared applications *Appl. Opt.* **36** 9075

[11] Gopal V and Harrington J A 2003 Deposition and characterization of metal sulfide dielectric coatings for hollow glass waveguides *Opt. Express* **11** 3182

[12] Ouzounov D G *et al* 2003 Generation of high-power, non-frequency shifted solitons in a gas-filled photonic band-gap fiber *CLEO/QELS* p QThPDA3

[13] White T P *et al* 2002 Multipole method for microstructured optical fibers. I. formulation *J. Opt. Soc. Am.* B **19** 2322

[14] Ferrando A *et al* 1999 Full vector analysis of a realistic photonic crystal fiber *Opt. Lett.* **24** 276

[15] Kuhlmey B T, McPhedran R C and deSterke C M 2002 Modal cutoff in microstructured optical fibers *Opt. Lett.* **27** 1684

[16] Fini J M 2003 Bloch theory describing cladding modes of microstructure optical fiber *ECOC* p We4.P.37

[17] Müller D *et al* 2003 Measurement of photonic band-gap fiber transmission from 1 to 3 μm and impact of surface mode coupling *CLEO/QELS* p QTuL2

[18] Saitoh K and Koshiba M 2003 Confinement losses in air-guiding photonic bandgap fibers *Photon. Technol. Lett.* **15** 236

[19] Wang Z and Ramachandran S 2003 Ultrasensitive long-period fiber gratings for broadband modulators and sensors *Opt. Lett.* **28** 2458

[20] Johnson S G *Mit Photonic bands* http://ab-initio.mit.edu/mpb
[21] Mortensen N A, Nielsen M D, Folkenberg J R, Hansen K P and Simonsen H R 2003 Improved large-mode-area endlessly single-mode photonic crystal fibers *Opt. Lett.* **28** 393
[22] Litchinitser N M *et al* 2002 Antiresonant reflecting photonic crystal optical waveguides *Opt. Lett.* **27** 1592
[23] Mortensen N A, Folkenberg J R, Nielsen M D and Hansen K P 2003 Modal cutoff and the v parameter in photonic crystal fibers *Opt. Lett.* **28** 1879
[24] Kong J A 1990 *Electromagnetic Wave Theory* (New York:Wiley)
[25] Eggleton B *et al* 1999 Grating resonances in air–silica microstructured optical fibers *Opt. Lett* **24** 1460